Structural Refinement, Core–Shell Electron Structure, Enhanced Phosphorescence, and Splitting of $^5D_0 \rightarrow {}^7F_2$ Transitions in Li-doped Rare Earth Oxide Systems

Riyas K M [a], Peediyekkal Jayaram [a*], Sreedevi [a], Prasoon Prasannan [b], Sona C P [a], Liudmila Khoroshko[c,d], Aleksey Baglov [c, d]

[a] Materials and Condensed Matter Physics Laboratory, Department of Physics, MES Ponnani College, Ponnani, Malappuram, Kerala, India

[b] Government Polytechnic College, Naduvil, Kerala, 670582

[c] Faculty of Physics, Belarusian State University, 4 Nezavisimosti Av., 220030 Minsk, Belarus

[d] R&D Department, Belarusian State University of Informatics and Radioelectronics, 6 P. Browka Str., 220013 Minsk, Belarus

Abstract

Various concentrations of Lithium-Europium doped Gadolinium Oxide powders are synthesized by a high-temperature solid-state reaction method. X-ray diffraction pattern of the compounds revealed single-phase crystal formation, consistent with the predominant monoclinic phase of Gd_2O_3. The scanning electron micrographs and their analysis showcase dense growth of microparticles with average sizes ranging between 1.5 to 2 μm. The presence of constituent elements was identified using X-ray photoelectron spectroscopy. Eu3*d*, Li1*s*, Gd4*d*, and O1*s*, spectra were detected using the narrow scan spectra, and their deconvolutions of them show valance stability in the compound systems. Deep-level photoluminescence spectra showed enhanced multiple emissions in the orange-red region corresponding to transitions of $^5D_0$-$^7F_2$, $^5D_0$-$^7F_1$, and $^5D_0$-$^7F_0$ arising from Lithium activator incorporation. Polarization anisotropy of the monoclinic structure of samples brought out interesting crystal field splitting in the pure electric dipole $^5D_0$-$^7F_2$ transitions.

Keywords: Phosphorescence, Rare earth Oxides, XPS, XRD, Photoluminescence

Corresponding author's email address: *jayarampnair@gmail.com

1. Introduction:

Modern photonics pays much more attention to the fabrication of rare earth luminescent materials which are tuneable for emission wavelengths by influencing lattice crystal field variations [1]–[3]. In-depth and diverse investigations are carried out to maximize the efficiency and fine-tune the emission wavelengths for these lanthanide phosphors because of their synthesis flexibility, low cost of production, long lifetime, etc. [4]–[6]. Enhancing the luminescence intensity of these lanthanide ions by suitable modification of host matrix structures has been a significant subject of investigation in recent years. Modification of lanthanoids' luminescence can be provided by the varying in their concentrations through ion-ion interaction[7] and by the embedding of co-activators ions likewise the non-lanthanide luminophores[8], but co-activation mechanisms will be different. Incorporating similar radii alkali ions into the host matrix creates interesting distortions in rare earth visible light emitter ion surroundings, favourable for higher intensity emissions in desired regions. This can be achieved by incorporating relaxing factors for selection rules that prevent the transitions of special interest. The electronic-dipole transitions among the states arising from 4f levels in lanthanide ions are forbidden by Laporte selection rules. However partial relaxations in these selection rules are permitted by the local crystal field around the lanthanide ions due to the capability to intermix with their states of odd parity [9]. Modification of the local crystal field around the lanthanide ions and thereby altering the radiative parameters is a promising strategy for improving the luminescence efficiency as the Li^+ ion possesses the smallest cationic radius in the periodical table of elements which is suitable for their mobility and site occupation in the host lattice. These advantages make them crucial activators for use in tailoring the host lattice's local crystal field [10]. In this work, we probe the emission intensity of Gd_2O_3:Eu^{3+} with the co-doped addition of Li^+ by a high-temperature solid-state reaction synthesis method. Emission intensity variations of the samples are deeply analysed with varying Li^+ dopant concentrations. In our previous work, we have reported the emission intensity enhancements due to various doping concentrations of Eu in one of the most prominent rare earth host matrix Gd_2O_3 [11], [12]. We found that 5% of Eu concentrations showed maximum intensity for emissions in the orange-red region. As a subsequent investigation in this work, we have synthesized our samples with fixed 5% Eu concentration and varying Li co-dopant concentrations. The structural and luminescent features of the prepared samples are thoroughly analysed. The presence of intensity variations in transitions which are supposed to be least sensitive to crystal surroundings are also deeply investigated.

2. Materials and Method:

Solid solutions of Eu-doped Gd_2O_3 powder samples were prepared by high-temperature solid-state reaction technique. The starting materials, Gd_2O_3 (Gadolinium Oxide, 99.99% purity), Eu_2O_3 (Europium Oxide, 99.99% pure), and Li_2O (Lithium Oxide 99.9% pure) were purchased from Sigma Aldrich Chemical Co. U.S.A. The powder samples were weighed in adequate quantities to obtain doping in weight percentages. The powders were mixed for 48–54 h to attain uniformity and were calcined initially at 1200 °C for 10–12 h. The samples were allowed to cool down naturally to room temperature after the calcination, and were reground into fine powders and loaded back into the furnace for the next round of heat treatment. The powders were then undergone for a step-by-step heating com grinding process between 1250 and 1400 °C for 60-65 h. The pellets were made from the powders and were densified at 1450^0C for 12 h and these pellets were reground and repellatized and then placed in the furnace for last round of heat treatment for 12 h at 1475 °C. The samples used for the study are finely ground powder after the final sintering process. The powder X-ray Diffraction (XRD) pattern was obtained using PANalytical, AERIS diffractometer calibrated by Cu-K_α-radiation of wavelength 1.5406 Å. X-ray photoelectron emission spectra were obtained by Prevac XPS equipment equipped with an MX650 monochromator. Scanning Electron Micrographs (SEM) recorded by VEGA-TESCAN 3 analyzer with EDAX arrangement. The UV- Spectra of the powders were recorded in diffuse reflectance mode by Perkin Elmer LAMBDA 365 UV–Vis Spectrophotometer. Photoluminescence (PL) measurements were carried out by JASCO FP-8300 spectrofluorometer.

3. Results and Discussions

3.1. X-ray diffraction analysis

Figure 1 shows the recorded XRD pattern of Gd_2O_3 doped with Eu (5%) and Li at different weight percentages varying from 4 to 12%. The reflections from the various lattice planes are indexed. The diffraction pattern of the planes indexed shows analogous to the typical monoclinic phase of Gd_2O_3 reported previously in ICCD : 98–016-0226 [11]. Most rare earth ions accept a large range of coordination numbers varying from 6 (octahedral) to 12 (dodecahedral) according to their ionic radii [13]. Gd_2O_3 crystallizes in the monoclinic C2/m space group. There are three inequivalent Gd^{3+} sites. In the first Gd^{3+} site, Gd^{3+} is bonded to six O^{2-} atoms to form a mixture of distorted corner and edge-sharing Gd-O_6 octahedra. In the second and third Gd^{3+} sites, Gd^{3+} is bonded in a 7-coordinate geometry to seven O^{2-} atoms but

differ in bond distances. Fragment of Gd_2O_3 structure with the described elements generated by VESTA are presented in the Figure.3. [14].

The Li^+ ions occupying the Gd^{3+} sites significantly have distorted the monoclinic structure which will favour enhanced luminescence. The Li^+ ions with higher concentrations occupy the interstitial sites rather than substitutional sites expands the lattice [15]. Thus, the leftward shift of XRD peaks for increasing concentrations of Li in our sample indicates the crystal lattice expansion. The average crystalline sizes calculated by Scherrer's equation are about 45–50 nm for different doping concentrations. It's found that the grain sizes of the lower concentration of Li contained samples are having lower grain sizes and higher dislocation density, which is also consistent with the SEM results shown in figure 5. This can happen in solid state reaction synthesis that normally arises due to the non-uniform grinding.

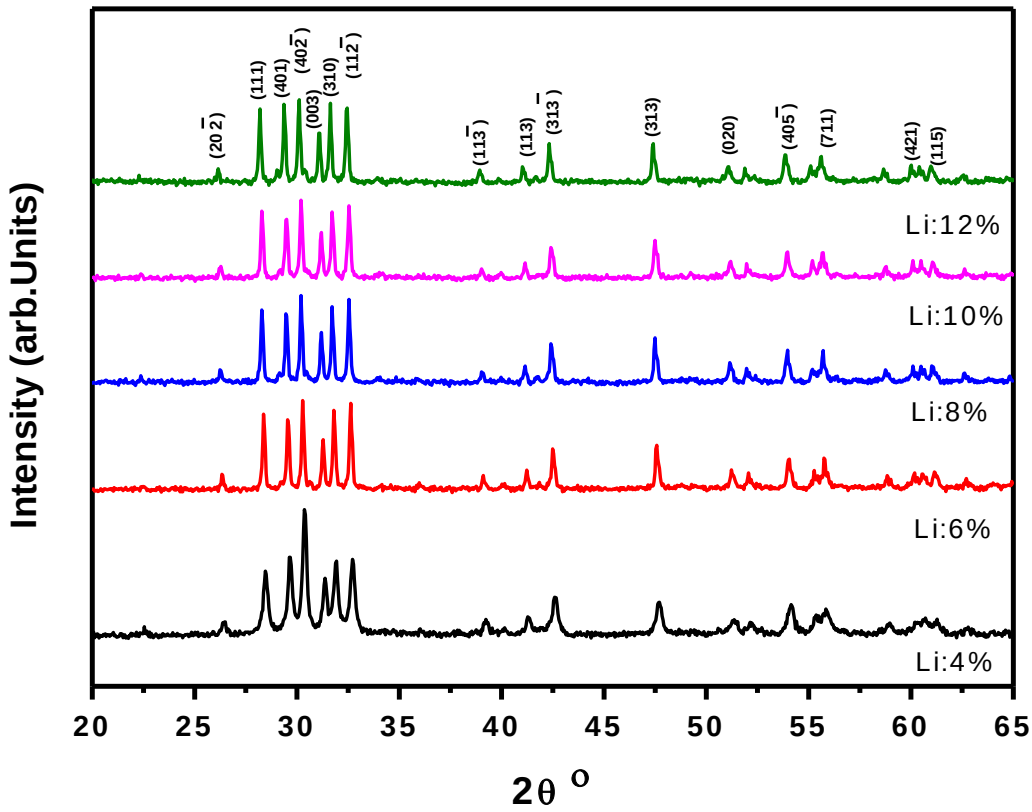

Figure.1. The X-ray diffraction pattern of the samples indicating phase purity with the orientations of planes from the monoclinic structure of Gd_2O_3

Lattice parameters of the monoclinic unit cells of the prepared sample are tabulated. A significant increase in the unit cell volume [16] is evident from the calculations. As the Li concentration is varied above 4%, all the unit cell parameters and unit cell volume seem to be increased. It indicates clearly the higher occupation of Li^+ ions in the interstitial sites. Such crystallographic distortions would bring the desired crystal field effects in the surroundings of

the emitter and thereby interesting transitions, which are generally forbidden, can happen as induced transitions by relaxing the selection rules [17].

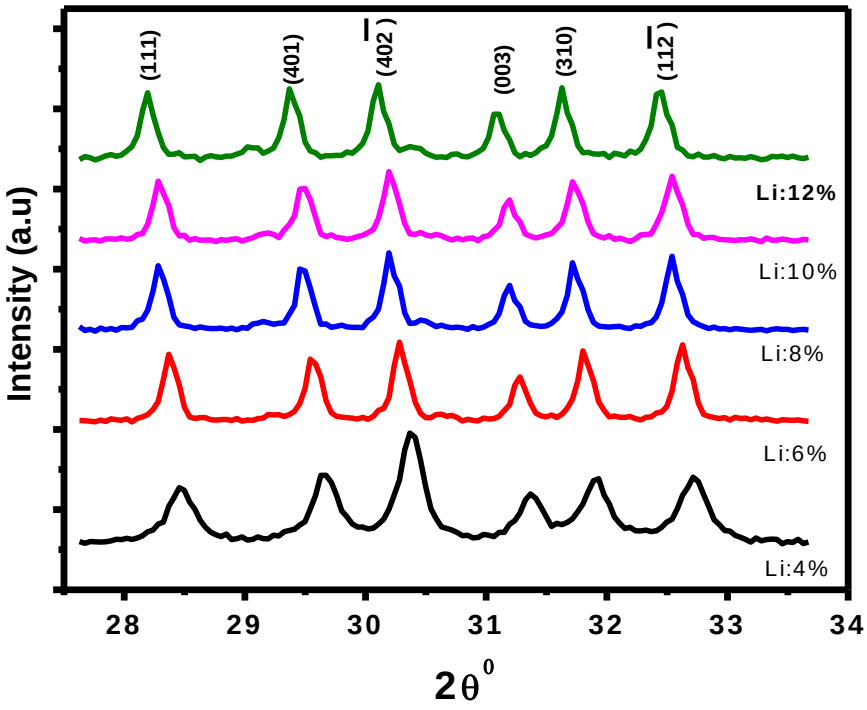

Figure.2. Magnified XRD pattern of the prominent reflections of monoclinic Li doped Gd_2O_3: Eu^{3+} (5%) in C2/m space group.

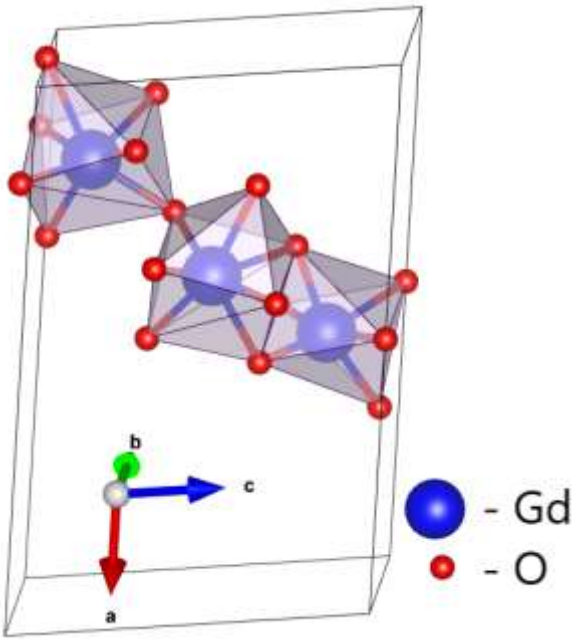

Figure. 3.Fragment of Gd_2O_3 crystalline structure

Figure 2 displays the magnified image of the prominent reflections form the samples, between the Brag angles 28 to 33^0. The image reveals that the characteristic reflection of monoclinic structure of Gd_2O_3 in maintained throughout the compositions and slight variation in speak positions are due to the possible structural asymmetry due to the substitutions of anions in the crystal matrix.

Table 1. The lattice parameters were calculated using the prominent reflections of the XRD pattern and the calculated sizes of the grains using the Scherrer formula, and the dislocation density was estimated [18].

Concentration	**a**	**b**	**c**	**V**	**Grain Size D (nm)**	**Dislocation density δ ($1/D^2$) (x $10^{14}m^{-2}$)**
Li 4%	12.11	4.35	9.42	451.71	35	8.16
Li 6%	12.15	4.36	9.45	454.95	64	2.44
Li 8%	12.18	4.37	9.47	458.45	68	2.16
Li10%	12.18	4.37	9.47	458.61	61	2.68
Li 12%	12.22	4.38	9.50	462.60	68	2.16

The Rietveld refinement was employed purely to confirm the monoclinic crystal structure of the as-synthesized sample[19]. The data points were refined using the FULLPROF program. Fig.4 represents the Rietveld refinement of the prepared Gd_2O_3: Eu5%: Li 6% sample. The experimental and stimulated XRD intensities are in agreement with each other. Rietveld refinement confirmed the monoclinic structure of the Gd2O3:Eu:Li with $\chi 2$ value 1.51[20].Refinement results also confirmed the phase purity of the samples. The Whykoff positions of the three inequivalent Gd^{3+} ions is 4i positions. Li+ ions seems to occupy the first Gd3+ ion position which is bonded to six O^{2-} atoms which forms a mixture of distorted corner and edge sharing GdO_6 octahedra without tilting[21].The lattice parameters calculated from XRD data were also in good agreement with the refinement data .The respective coordinates of atomic positions are listed in table 2.

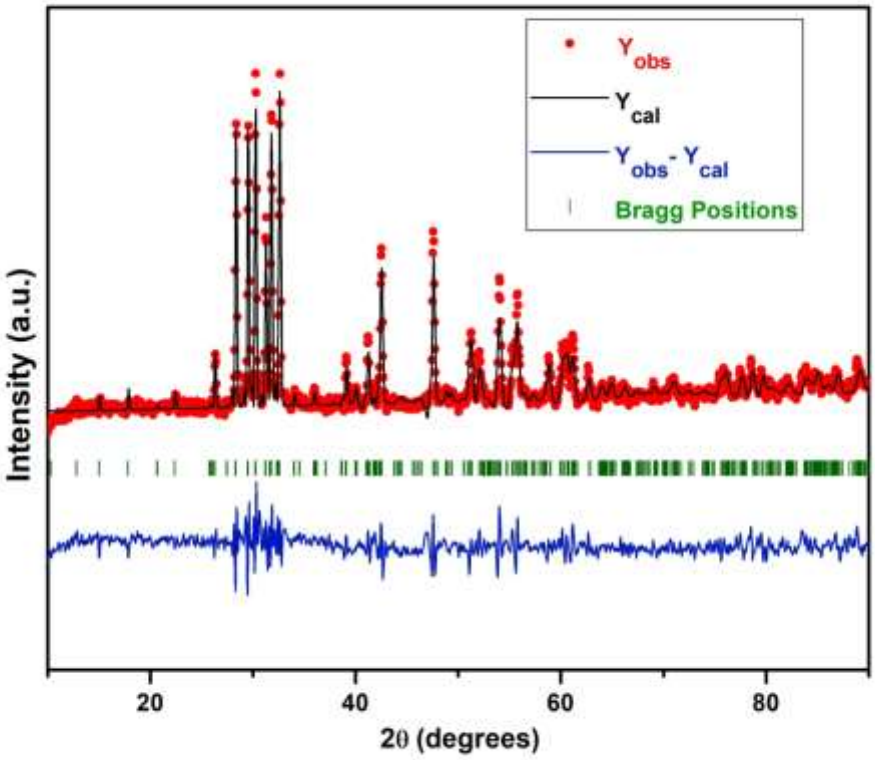

Figure 4. Rietveld Refined plot of Gd_2O_3: Eu5%: Li 6% sample

Table 2. Calculated lattice positions of atoms in the monoclinic matrix of Gd2O3 host matrix

Name	X	Y	Z
Gd1/Li1	0.03187	0.81098	0.50000
Gd2/Eu1	0.1356	0.48980	0.50000
Gd3	0.19028	0.13415	0.50000
O3	0.00093	0.63292	0.50000
O4	0.13797	0.28989	0.50000
O5	0.19122	0.98594	0.50000
O6	0.20482	0.64984	0.50000
O7	0.00000	0.00000	0.25000

3.2. Surface Morphology and Chemical Composition

3.2.1. Scanning Electron Micrographs

The SEM images of the as-prepared samples Gd_2O_3:Eu^{3+} co-activated with 4%, 6%, 8%, 10% and 12% concentrations of Li are shown in Fig 3 (a), (b), (c), (d) and (e) respectively. In the figure, it found that the sample was composed of non-uniform spherical-shaped particles. Fig 5 (a) is the SEM image of a 4% Li doped sample, in which the surface of the sample was

found to be rougher than the images of the other samples. As the concentration of Li increases the agglomeration of the particle can be observed in the SEM images. The Fig 5 (c) & (d), sample with 8% and 10% respectively, shows more agglomeration than other samples. This indicates that there is no trend has been followed for agglomeration, so we could conclude that the agglomeration could be due to the non-uniform grinding[22].

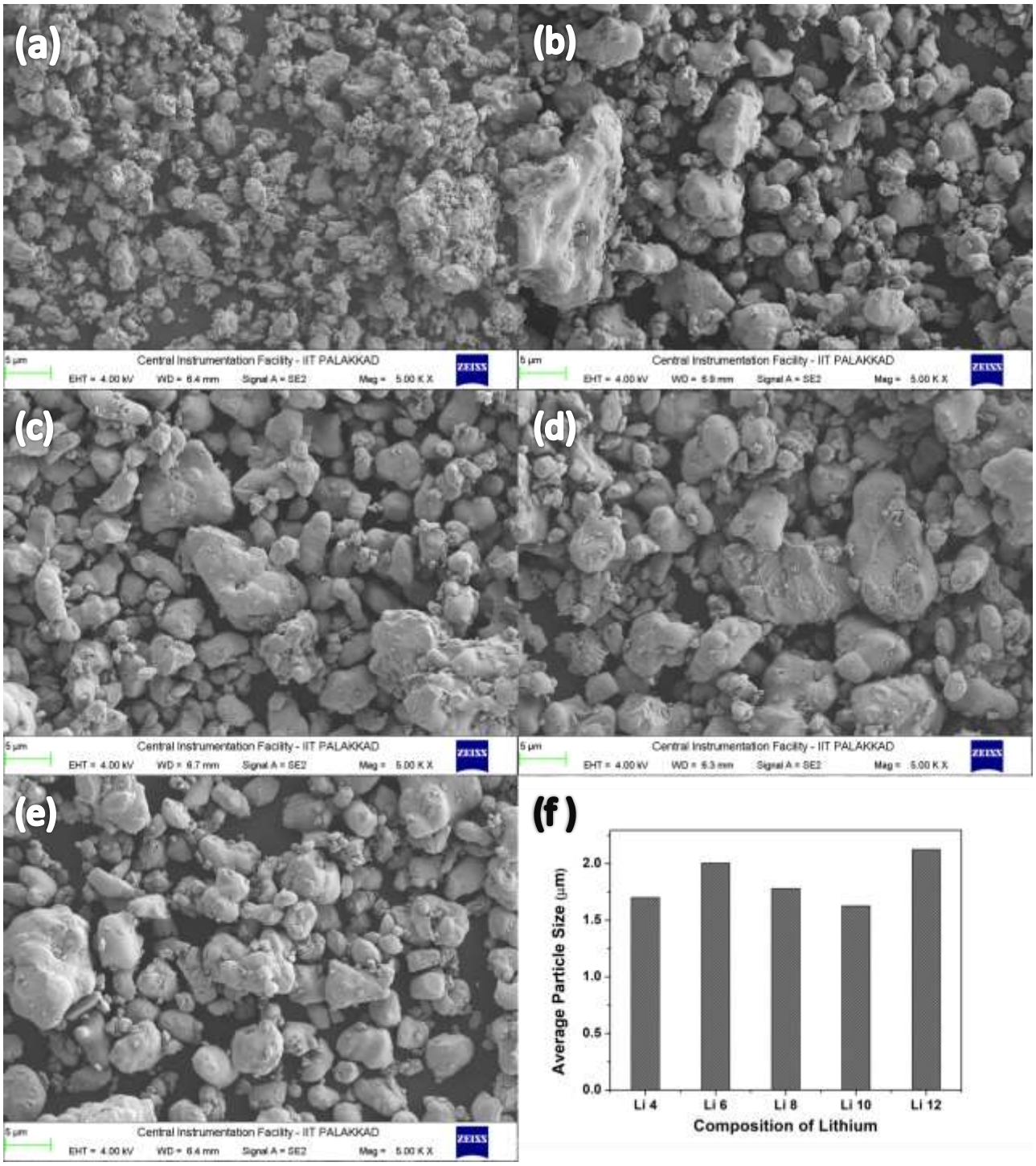

Figure 5, Scanning Electron Micrographs of a) Li 4% $Gd_2O_3:Eu^{3+}$ b) Li 6% $Gd_2O_3:Eu^{3+}$ c) Li 8% $Gd_2O_3:Eu^{3+}$ d) Li 10% $Gd_2O_3:Eu^{3+}$ e) Li 12% $Gd_2O_3:Eu^{3+}$ and (f) Bar diagram showing average particle size of different composition of Li

Fig 5 (f) shows a bar diagram indicating the average particle size of $Gd_2O_3:Eu^{3+}$ co-doped with different concentration lithium oxides, the average particle size was calculated by

collecting 60 clearly identifiable particles for each concentration found to be 1.70 μm, 2.00 μm, 2.084μm, 1.62 μm and 2.12 μm for 4%, 6%, 8%, 10% and 12% respectively. The average crystallite size calculated using the Debye Scherer formula from XRD data and the average particle size estimated from SEM are differ by a factor of 10^{-2}. Since the average crystallite size represents the average size of the coherently diffracted domains and the average particle size observed in SEM is the apparent size of the particle [23]. This infers that the sample is the polycrystalline micro particle. Figure 6 displays the histogram of the particle sizes observed in measurements which was used for the plotting figure 5(f).

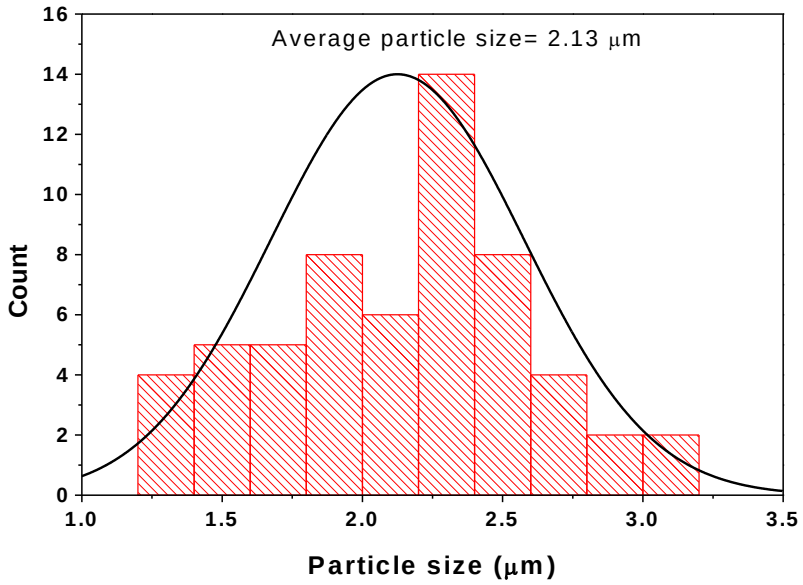

Figure.6. The histogram representing average particle sizes measured on the scanning micrograph of Li 4% Gd_2O_3:Eu^{3+} powder samples

3.2.2. X-ray photoelectron spectroscopy

The presence of constituent elements in the prepared materials is identified using X-ray photoelectron spectroscopy (XPS). Figure 7 represents the core level elemental XPS spectra of Gd_2O_3 doped with Eu (5%) and Li at 6%. The obtained asymmetric curves are deconvoluted for the appropriate electronic states and the results are interpreted using the NISTXPS database [24]. As displayed in the Figure 7 all elements constitute significant peak asymmetry and fitted their corresponding components. The elemental photoelectron emissions of Eu*3d* and Gd*4d* were due to the energy states of the and the split up is due to the J-J coupling [25]. The detected broad spectra between the binding energy region 1127-1143 eV (figure 7.a), are from Eu*3d* binding energy state and comprise strong peak asymmetry. This was fitted with two Gaussian-Lorentzian components at positions 1136.2 ± 0.05 eV due to Eu $3d_{5/2}$ and 1132.0 ± 0.05 eV being Eu$3d_{3/2}$ energy states [24]. The typical peak difference (ΔV) between Eu *3d* coupling constant is 4.2eV and is exactly re-produced here [16]. Gd *4d*

in Fig. 7.b, the doublets in 140.59 ± 0.05 eV and 145.20 ± 0.05 eV, are respectively from Gd $4d_{3/2}$ and Gd $4d_{5/2}$ split ups, and the emissions are from Gd^{3+} ionic state with oxygen. it can be a remark for the Gd^{3+} electronic state alongside ΔV = 5.01eV also consistent with references [26]. Consequent to the changes in doping concentration, observed a slight variation in the peak positions, for all elements however the shapes of the peaks remain unchanged and hence all the cations possess valance stability [27]. O *1s* spectra in multi-cation oxide systems are typically broad, with an obvious peak-shape asymmetry due to distinct ionic interactions with multiple cations, metal carbonates, and hydroxyls that are naturally present in any chemical [28]. The O*1s* photoelectron peak showed a strong emission with shoulder peak, mainly due to the presence of two components at binding energy values of 530.78 ± 0.05 eV and 528.36 ± 0.05 eV corresponds to the bond between O^{2-} - Eu^{3+} and O^{2-}-Gd^{3+} states [29] . The broad spectrum that was obtained between 53 and 56 eV is consistent with the Li 1s emission, and it fit two components: Li-C bonds and Lithium with oxygen bonds[30].

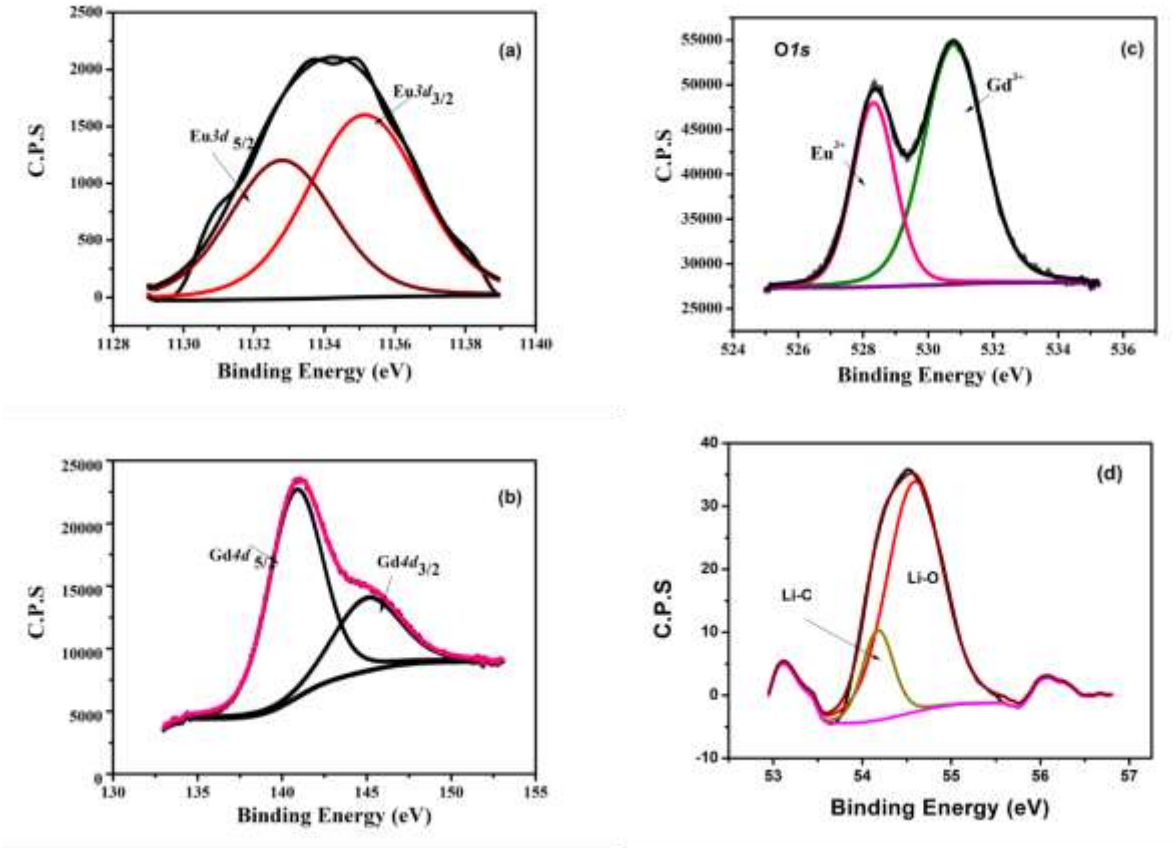

Figure 7. The core-level XPS spectra of the sample recorded in the narrow scan mode (a) Eu 3d state (b) Gd 4d state (c) O 1s state and (d) Li 1s

3.3.Photoluminescence studies

Photoluminescence emission spectra of the samples with Eu concentration fixed at 5% and Li concentration varied from 4% to 12% are depicted in Figure 8. The emission spectra reveal significant efficiency improvement resulting from Li^+ doping, in the visible region of Eu^{3+} emissions. Our specific interest of emission region is 570nm -710 nm. Five possible transitions in this region are between the energy levels $^5D_0$-$^7F_0$, $^5D_0$-$^7F_1$, $^5D_0$-$^7F_2$, $^5D_0$-$^7F_3$, and $^5D_0$-$^7F_4$. They are ED, MD, ED, ED and ED transitions respectively, where ED indicates electric dipole transition and MD indicates magnetic dipole transitions [17]. In these energy states and corresponding transitions, parity selection rules demand that the transitions between states with same parity have is prohibited for electric dipole transitions; as a consequence, f–f transitions are forbidden by the ED mechanism[31]. However, under the influence of a ligand field, the lanthanide ions' non-Centro symmetric interactions allow the mixing of electronic states of opposite parity into the 4f wavefunctions, which dilutes the selection rules, and the transitions become partially allowed; and are termed as induced (or forced) electric dipole transitions. Certain induced ED transitions are extremely sensitive to minute distortions in the Ln^{3+} surroundings and are considered to be hypersensitive [32]. The very presence of $^5D_0$-$^7F_0$ transition at 578 nm indicates the placing of emitter Eu^{3+} at C_s or C_2 symmetry sites[33]. The ground state ($^7F_0$) and the most important emitting excited state ($^5D_0$) are non-degenerate and are thus not split by the crystal-field effect[34]. However, the relative intensity of this emission compared with other prominent transitions seems to be very low in our samples. The addition of Li^+ also hasn't improved the intensity of this transition to any considerable level. It indicates that the increasing presence of Li^+ ions which resulted in crystallite distortions could not bring linear contribution to the crystal field Hamiltonian, which enhances the particular emission intensity, as reported by X Y Chen et al [35]. The $^5D_0 \rightarrow ^7F_1$ emission transitions within the range 585–600 nm show slight increase as Li^+ concentration is increased. This transition is a magnetic dipole (MD) transition[35]. The intensity of an MD transition is mostly independent of the surroundings of the lanthanide. In other words, the kind of ligands present or the specific symmetry of the coordination polyhedron in the surroundings of the lanthanide ion does not influence the MD intensity largely[36]. However, our sample shows a notable increase in intensity for this emission. This is aroused from the high level of J-mixing resulting due to the wavefunction overlapping close to this energy region [37].The multiple peaks observed in these regions reinstates the crystal field splitting of this transition for three components as predicted by Binnemans et al [38]. Those three peaks are observed at 582, 591 and 595 nm. The trend of emission intensity variation for this transition with an increase in Li^+ concentration seems to be similar to the intensity variation trend shown by the $^5D_0$-$^7F_2$ transition emission for our samples.

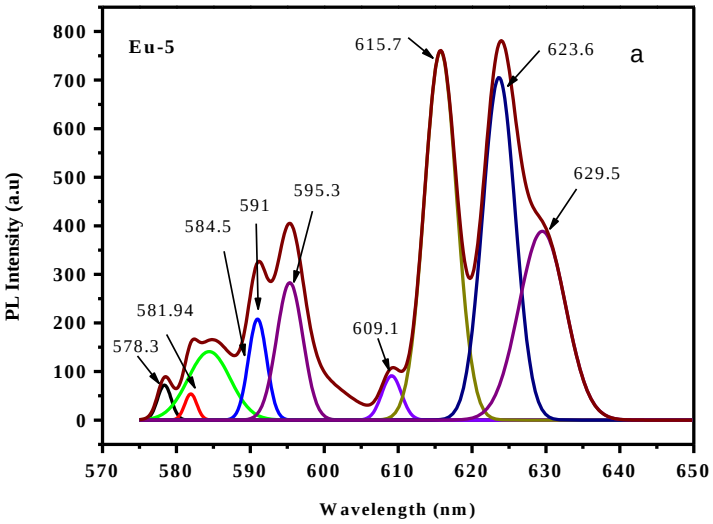
Eu-5
a
PL Intensity (a.u)
Wavelength (nm)
615.7
623.6
629.5
595.3
591
584.5
581.94
578.3
609.1

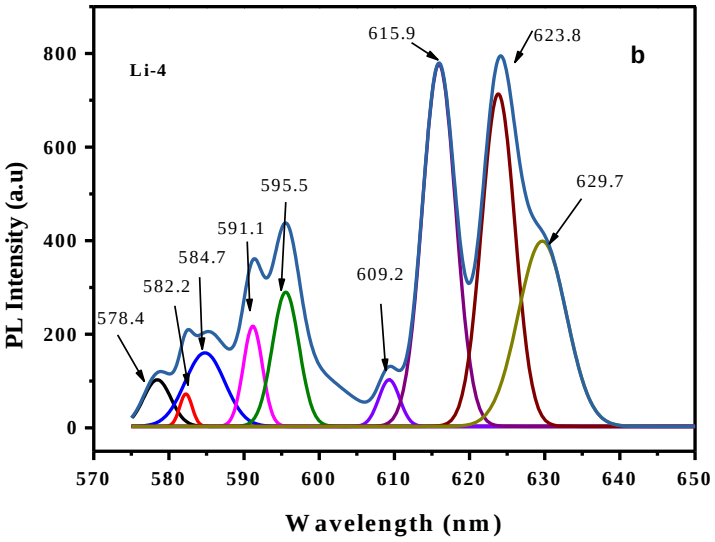
Li-4
b
PL Intensity (a.u)
Wavelength (nm)
615.9
623.8
629.7
595.5
591.1
584.7
582.2
578.4
609.2

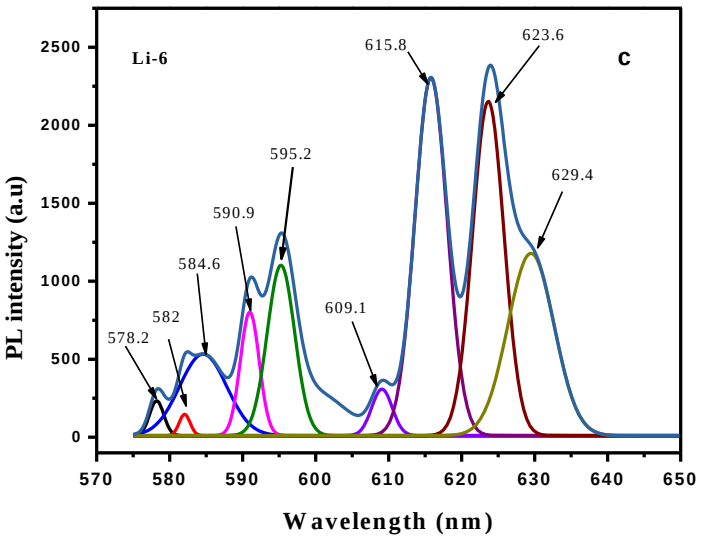
Li-6
c
PL intensity (a.u)
Wavelength (nm)
615.8
623.6
629.4
595.2
590.9
584.6
582
578.2
609.1

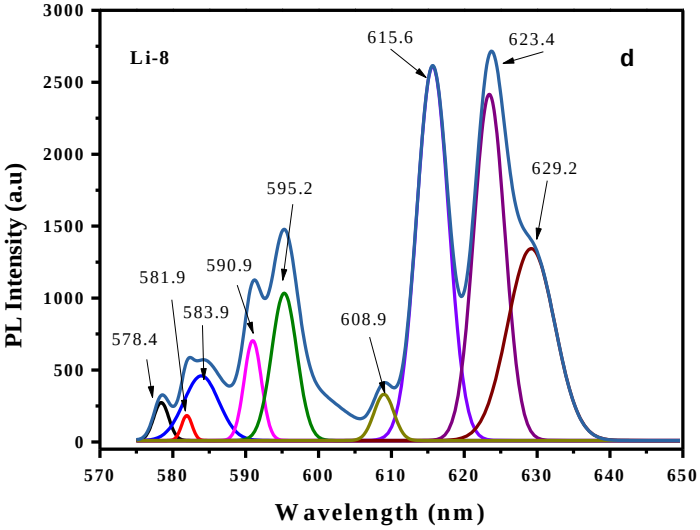
Li-8
d
PL Intensity (a.u)
Wavelength (nm)
615.6
623.4
629.2
595.2
590.9
583.9
581.9
578.4
608.9

e

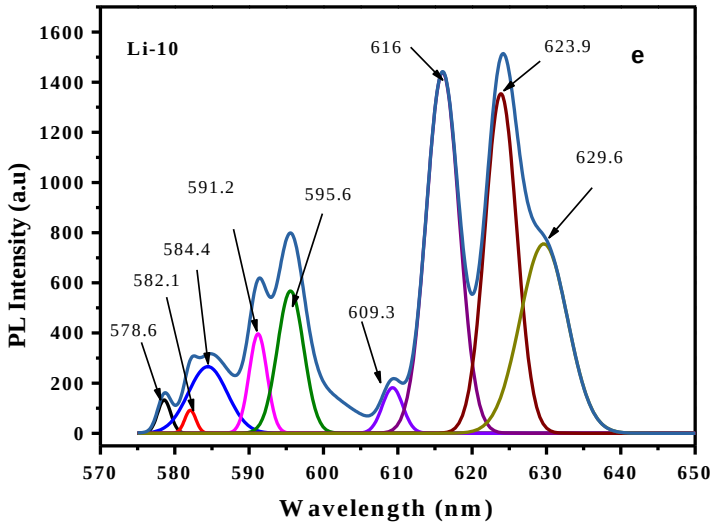
Li-10
e
PL Intensity (a.u)
Wavelength (nm)
616
623.9
629.6
595.6
591.2
584.4
582.1
578.6
609.3

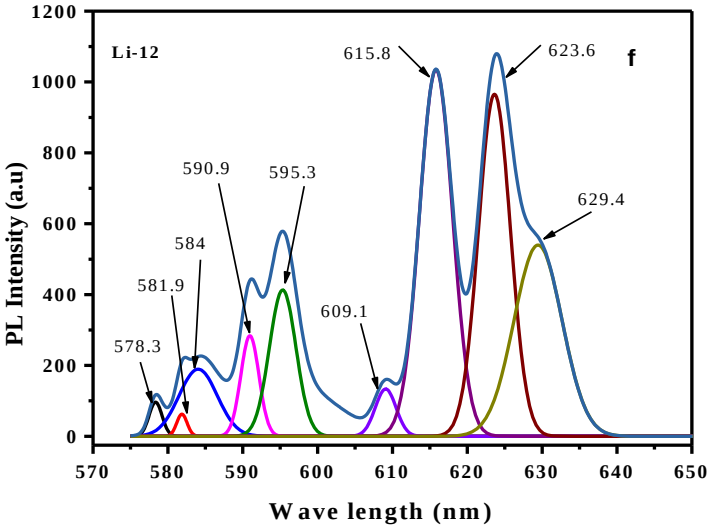
Li-12
f
PL Intensity (a.u)
Wave length (nm)
615.8
623.6
629.4
595.3
590.9
584
581.9
578.3
609.1

Figure .8. Deconvoluted (Gaussian peak type) PL spectra of Eu doped Gd_2O_3 which was previously reported as the superior colour emission when doping concentration reaches 5% and figures a.b.c.d and f are the deconvoluted photoluminescence spectra of Li co-doped Gd_2O_3 microphosphers synthesized at different concentrations of Li-ions

The intensity is found maximum for 8% doping of Li. The deconvoluted spectrum indicates the fact that the crystal field splitting for this transition for our sample is 3. $^5D_0$-$^7F_2$ transitions, with the wavelength range of 610–630 nm are electric dipole transitions and are hypersensitive to the crystal field environments[39]. That is its intensity is highly influenced by the local symmetry around the Eu^{3+} ion and the ligand nature than the intensities of the other ED transitions. The intensity of these transitions in our samples shows very interesting improvements with the addition of Li. As the Li concentration is varied from 4% to 12%, by steps of 2%, the emission intensity for this transition first increases and then decreases. Intensity is found to be maximum for 8% Li doping concentrations and found to have improved by 75% than without Li dopant. The dominance of this $^5D_0$-$^7F_2$ transition over $^5D_0$-$^7F_1$ clearly indicates the absence of centre of inversion in the sample crystal structure [40]. The deconvoluted spectrum reveals the fact that the crystal field splitting for this transition, $^5D_0$-$^7F_2$, for our sample is 4. Those 4 emissions are situated at 609.1, 615.7, 623.6 and 629.5 nm. All these four emissions are the results of polarisation anisotropy for this particular monoclinic structure of our sample. Their respective positions are at 609, 616, 623 and 629 nm. Out of these four transitions, emission at 616 and 623 shows maximum intensity enhancement for Li concentration variations. The overall analysis of crystal field splitting of these three prominent transitions reveals the point C_{2V} point group formation around Eu^{3+} as reported by X Qin et al. [40].

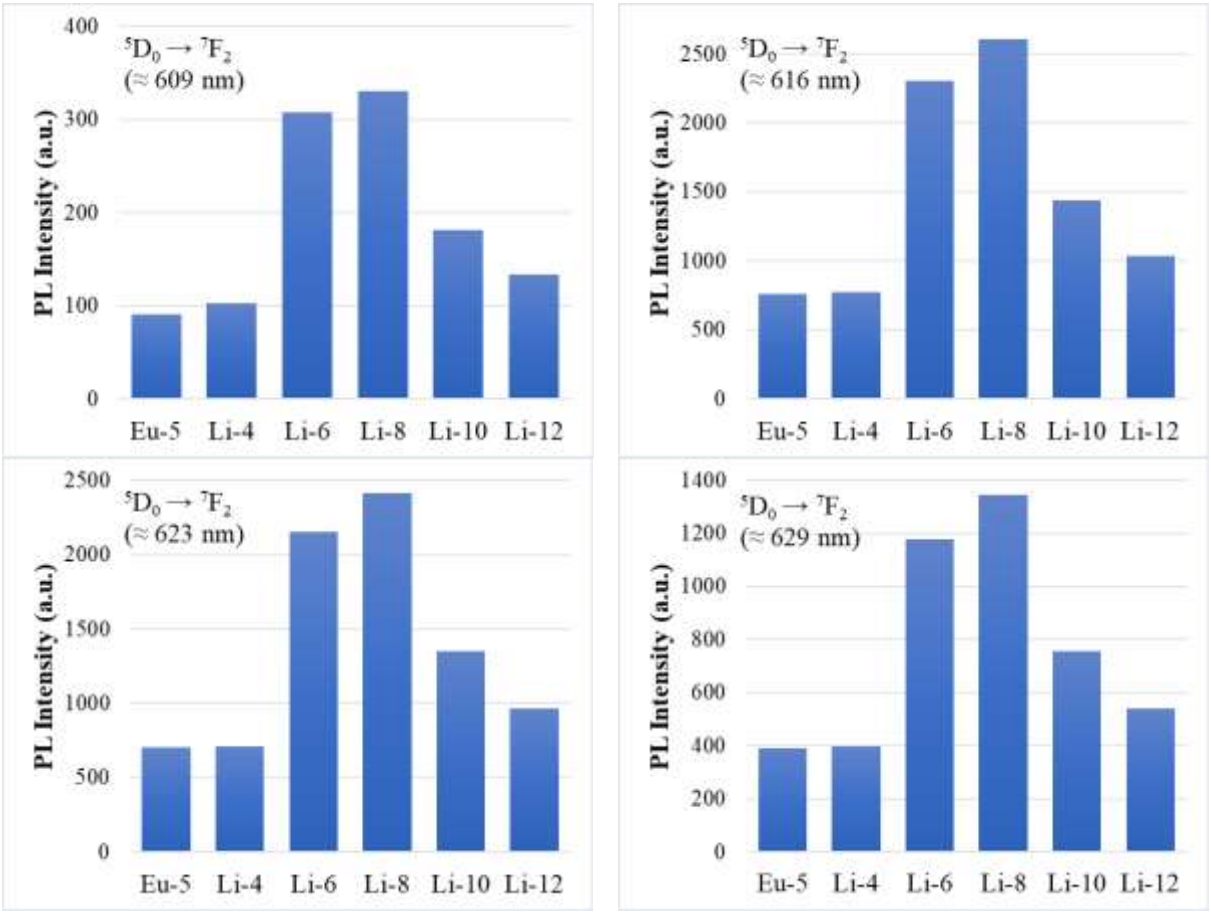

Figure.7. Change in the luminescence intensity of the $^5D_0 \rightarrow {}^7F_2$ of Eu^{3+} in the Gd_2O_3 with different Li concentrations according to the deconvoluted peaks of photoluminescence spectra

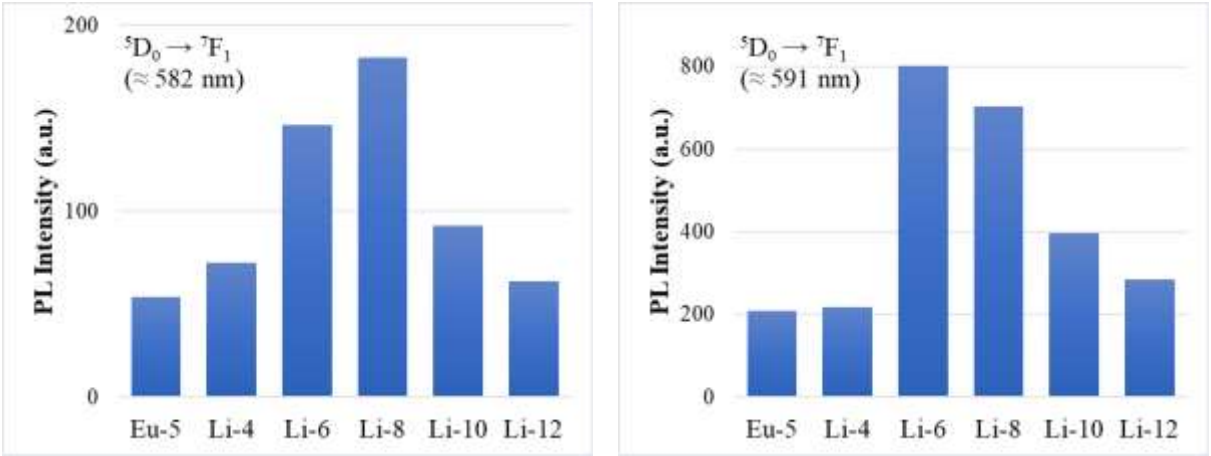

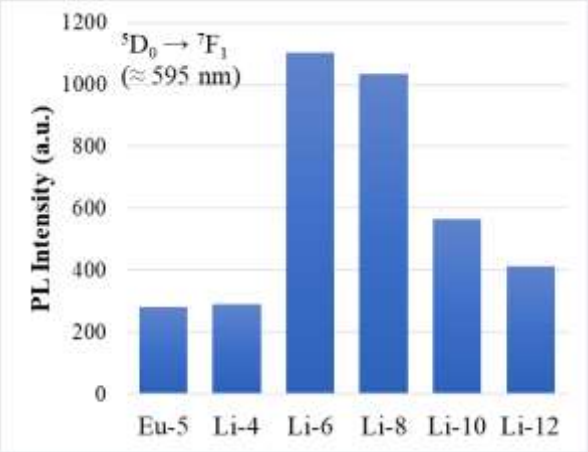

Figure. 8. Change in the luminescence intensity of the $^5D_0 \rightarrow {}^7F_1$ of Eu^{3+} in the Gd_2O_3 with different Li concentrations according to the deconvoluted peaks of photoluminescence spectra.

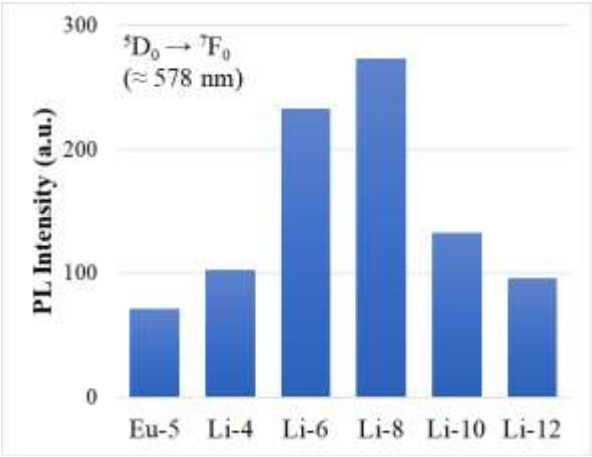

Figure. 9. Change in the luminescence intensity of the $^5D_0 \rightarrow {}^7F_0$ of Eu^{3+} in the Gd_2O_3 with different Li concentrations according to the deconvoluted peaks of photoluminescence spectra.

The histograms depicted in figures 7 to 9 clearly portraits the intensity enhancement due to the addition of activator Li in Gd_2O_3 microphosphers for the three major transitions in yellow- red region[41] [42]. Figure 8 shows, From figure.8, the peak at 592 nm demonstrate similar behavior to the $^5D_0 \rightarrow {}^7F_2$ luminescence, but the maximum of intensities of two other peaks is observed for the 6 % of Li concentration. The most intense emission wavelength for $^5D_0 \rightarrow {}^7F_2$ transition, 616nm shows almost 5 times enhancement for the Li8% dopant concentration than without Li incorporation. It clearly indicates the successful symmetry distortions and thereby formation of crystal field variations favourable for enhanced emissions of Eu^{3+} in red region.

4. Conclusions

The phase pure compounds composed of different percentage of Li^+ ions substituted in the monoclinic $Gd_2O_3:Eu^{3+}$ has been successfully synthesized by solid state reaction technique. The structural parameters were deduced and monoclinic features are depicted. The electronic state of the elements in the compound system was investigated and reported. The valence stability in the compound system was identified by peak shape analysis of elements scanning by XPS spectra. Photoluminescence analysis brought out the multiple intense color emissions in the orange-red region and deep analysis brought out the crystal field splitting in the emissions. Enhancement in emission intensities for Li^+ concentration variations is also reported. The study summarizes the emission enhancements and crystal field splitting as a result of favourable asymmetric crystal atmosphere around our Eu^{3+} emitter due to the systematic incorporation of Li^+ activators. Owing to the tuneable intensity of the Eu luminescence $Gd_2O_3:Eu^{3+}$ composites co-activated with Li^+ can be promising for use in electroluminescent appliances, field emission displays, biosensors, MRI contrast agents, and customizable converters of UV emission to visible luminescence.

REFERENCES

[1] S. Hu, J. Yang, C. Li, and J. Lin, 'Synthesis and up-conversion white light emission of RE3+-doped lutetium oxide nanocubes as a single compound', *Mater. Chem. Phys.*, vol. 133, no. 2–3, pp. 751–756, 2012.

[2] B. V. Ratnam, M. Jayasimhadri, K. Jang, H. Sueb Lee, S.-S. Yi, and J.-H. Jeong, 'White light emission from NaCaPO4: Dy3+ phosphor for ultraviolet-based white light-emitting diodes', *J. Am. Ceram. Soc.*, vol. 93, no. 11, pp. 3857–3861, 2010.

[3] Z. Pan, Y.-Y. Lu, and F. Liu, 'Sunlight-activated long-persistent luminescence in the near-infrared from Cr3+-doped zinc gallogermanates', *Nat. Mater.*, vol. 11, no. 1, Art. no. 1, Jan. 2012, doi: 10.1038/nmat3173.

[4] F. Wang *et al.*, 'Simultaneous phase and size control of upconversion nanocrystals through lanthanide doping', *nature*, vol. 463, no. 7284, pp. 1061–1065, 2010.

[5] S. K. Singh, K. Kumar, and S. B. Rai, 'Diode laser pumped Gd 2 O 3: Er 3+/Yb 3+ phosphor as optical nano-heater', *Appl. Phys. B*, vol. 100, pp. 443–446, 2010.

[6] G. A. Kumar, M. Pokhrel, A. Martinez, and D. K. Sardar, 'Synthesis and upconversion spectroscopy of Yb Er doped M2O2S (M= La, Gd, Y) phosphors', *Sci. Adv. Mater.*, vol. 4, no. 5–6, pp. 623–630, 2012.

[7] A. Podhorodecki *et al.*, 'Ion–ion interaction in two-dimensional nanoporous alumina filled with cubic YAlO3: Tb3+ matrix', *J. Phys. Appl. Phys.*, vol. 46, no. 35, p. 355302, 2013.

[8] K. A. Petrovykh *et al.*, 'Photoluminescence of the nanosized xerogel Zn2SiO4:Mn2+ in pores of anodic alumina', *Phys. Solid State*, vol. 58, no. 10, pp. 2062–2067, Oct. 2016, doi: 10.1134/S1063783416100280.

[9] M. J. Weber, 'Radiative and multiphonon relaxation of rare-earth ions in Y 2 O 3', *Phys. Rev.*, vol. 171, no. 2, p. 283, 1968.

[10] Q. Dou and Y. Zhang, 'Tuning of the structure and emission spectra of upconversion nanocrystals by alkali ion doping', *Langmuir*, vol. 27, no. 21, pp. 13236–13241, 2011.

[11] J. P and P. Prasannan, 'Multiple Deep-Level defect correlated emissions and phosphorescence in Eu3+ doped Gd2O3 Compound Systems', *Mater. Lett.*, vol. 273, May 2020, doi: 10.1016/j.matlet.2020.127925.

[12] K. M. Riyas and J. Peediyekkal, 'Lattice dynamics, core–shell electron structure and Judd − Ofelt analysis on europium-doped Gd2O3 micro phosphors', *J. Aust. Ceram. Soc.*, vol. 59, no. 3, pp. 769–778, Jul. 2023, doi: 10.1007/s41779-023-00873-z.

[13] B. Wu, M. Zinkevich, F. Aldinger, D. Wen, and L. Chen, 'Ab initio study on structure and phase transition of A- and B-type rare-earth sesquioxides Ln2O3 (Ln=La–Lu, Y, and Sc) based on density function theory', *J. Solid State Chem.*, vol. 180, no. 11, pp. 3280–3287, Nov. 2007, doi: 10.1016/j.jssc.2007.09.022.

[14] K. Momma and F. Izumi, 'VESTA 3 for three-dimensional visualization of crystal, volumetric and morphology data', *J. Appl. Crystallogr.*, vol. 44, no. 6, Art. no. 6, Dec. 2011, doi: 10.1107/S0021889811038970.

[15] N. Dhananjaya, H. Nagabhushana, B. M. Nagabhushana, B. Rudraswamy, C. Shivakumara, and R. P. S. Chakradhar, 'Effect of Li+-ion on enhancement of photoluminescence in Gd2O3:Eu3+ nanophosphors prepared by combustion technique', *J. Alloys Compd.*, vol. 509, no. 5, pp. 2368–2374, Feb. 2011, doi: 10.1016/j.jallcom.2010.11.023.

[16] D. A. Zatsepin *et al.*, 'Electronic structure, charge transfer, and intrinsic luminescence of gadolinium oxide nanoparticles: Experiment and theory', *Appl. Surf. Sci.*, vol. 436, pp. 697–707, Apr. 2018, doi: 10.1016/j.apsusc.2017.12.086.

[17] K. Binnemans, 'Interpretation of europium(III) spectra', *Coord. Chem. Rev.*, vol. 295, pp. 1–45, Jul. 2015, doi: 10.1016/j.ccr.2015.02.015.

[18] H. P. Klug and L. E. Alexander, 'Quantitative Analysis of Powder Mixtures in "X-ray Diffraction Procedures"'. Wiley and Sons, New York, 1954.

[19] L. B. McCusker, R. B. Von Dreele, D. E. Cox, D. Louër, and P. Scardi, ‘Rietveld refinement guidelines’, *J. Appl. Crystallogr.*, vol. 32, no. 1, pp. 36–50, 1999.
[20] M. Lang *et al.*, ‘Swift heavy ion-induced phase transformation in Gd2O3’, *Nucl. Instrum. Methods Phys. Res. Sect. B Beam Interact. Mater. At.*, vol. 326, pp. 121–125, May 2014, doi: 10.1016/j.nimb.2013.10.073.
[21] ‘mp-643084: Gd2O3 (Monoclinic, C2/m, 12)’, Materials Project. Accessed: Nov. 07, 2023. [Online]. Available: https://next-gen.materialsproject.org/materials/mp-643084#summary
[22] R. K. Tamrakar, D. P. Bisen, and N. Brahme, ‘Comparison of photoluminescence properties of Gd2O3 phosphor synthesized by combustion and solid state reaction method’, *J. Radiat. Res. Appl. Sci.*, vol. 7, no. 4, pp. 550–559, Oct. 2014, doi: 10.1016/j.jrras.2014.09.005.
[23] E. W. Awin, S. Sridar, R. Shabadi, and R. Kumar, ‘Structural, functional and mechanical properties of spark plasma sintered gadolinia (Gd2O3)’, *Ceram. Int.*, vol. 42, no. 1, Part B, pp. 1384–1391, Jan. 2016, doi: 10.1016/j.ceramint.2015.09.080.
[24] H. Bruncková, M. Kaňuchová, H. Kolev, E. Múdra, A. Kovalčiková, and Ľ. Medvecký, ‘X-ray Photoelectron Spectroscopy Study of Europium Niobate Thin Film Prepared by Chemical Solution Deposition’, *Powder Metall. Prog.*, vol. 20, no. 2, pp. 94–103, Dec. 2020, doi: 10.2478/pmp-2020-0009.
[25] P. Jayaram, P. P. Pradyumnan, and S. Z. Karazhanov, ‘Micro-strain, dislocation density and surface chemical state analysis of multication thin films’, *Phys. B Condens. Matter*, vol. 501, pp. 140–145, 2016.
[26] Y. Li, N. Chen, J. Zhou, S. Song, Z. Yin, and C. Cai, ‘Effect of the oxygen concentration on the properties of Gd2O3 thin films’, *J. Cryst. Growth*, vol. 265, no. 3–4, pp. 548–552, 2004.
[27] C. Le Luyer, A. García-Murillo, E. Bernstein, and J. Mugnier, ‘Waveguide Raman spectroscopy of sol-gel Gd $_2$ O $_3$ thin films: Sol-gel Gd $_2$ O $_3$ thin films’, *J. Raman Spectrosc.*, vol. 34, no. 3, pp. 234–239, Mar. 2003, doi: 10.1002/jrs.980.
[28] T. R. Felthouse, P. B. Fraundorf, R. M. Friedman, and C. L. Schosser, ‘Expanded lattice ruthenium pyrochlore oxide catalysts I. Liquid-phase oxidations of vicinal diols, primary alcohols, and related substrates with molecular oxygen’, *J. Catal.*, vol. 127, no. 1, pp. 393–420, 1991.
[29] D. Raiser and J. P. Deville, ‘Study of XPS photoemission of some gadolinium compounds’, *J. Electron Spectrosc. Relat. Phenom.*, vol. 57, no. 1, pp. 91–97, 1991.
[30] J. P. Contour, A. Salesse, M. Froment, M. Garreau, J. Thevenin, and D. Warin, ‘Analysis by electron-microscopy and XPS of lithium surfaces polarized in anhydrous organic electrolytes’, *J. Microsc. Spectrosc. Electron.*, vol. 4, no. 4, pp. 483–491, 1979.
[31] L. Smentek and A. Kędziorski, ‘f↔ f electric dipole transitions; old problems in a new light’, *J. Alloys Compd.*, vol. 488, no. 2, pp. 586–590, 2009.
[32] J.-C. G. Bünzli, ‘Lanthanide Luminescence: From a Mystery to Rationalization, Understanding, and Applications’, in *Handbook on the Physics and Chemistry of Rare Earths*, vol. 50, Elsevier, 2016, pp. 141–176. doi: 10.1016/bs.hpcre.2016.08.003.
[33] L. Smentek, B. G. Wybourne, and B. A. Hess Jr, ‘Judd–Ofelt theory in a new light on its (almost) 40th anniversary’, *J. Alloys Compd.*, vol. 323, pp. 645–648, 2001.
[34] J. Hölsä and P. Porcher, ‘Crystal field effects in REOBr: Eu3+’, *J. Chem. Phys.*, vol. 76, no. 6, pp. 2790–2797, 1982.
[35] X. Y. Chen and G. K. Liu, ‘The standard and anomalous crystal-field spectra of Eu3+’, *J. Solid State Chem.*, vol. 178, no. 2, pp. 419–428, Feb. 2005, doi: 10.1016/j.jssc.2004.09.002.
[36] O. A. Serra and L. C. Thompson, ‘Emission spectra of cesium sodium europium chloride (Cs2NaEuCl6) and cesium sodium europium yttrium chloride (Cs2Na(Eu,Y)Cl6)’, *Inorg. Chem.*, vol. 15, no. 3, pp. 504–507, Mar. 1976, doi: 10.1021/ic50157a002.

[37] P. Paufler, ‘KA Gschneidner, Jr., L. Eyring (eds.). Handbook on the Physics and Chemistry of Rare Earths, Vol. 16. North–Holland, Amsterdam 1993. 589 S. Preis US\pounds 309.50/Dfl. 420.75. ISBN 0–444–89782–8’. Wiley Online Library, 1995.
[38] K. Binnemans *et al.*, ‘Probing the Magnetic Anisotropy of Lanthanide-Containing Metallomesogens by Luminescence Spectroscopy’, *ChemPhysChem*, vol. 2, no. 11, pp. 680–683, 2001.
[39] C. Görller-Walrand and K. Binnemans, ‘Spectral intensities of ff transitions’, *Handb. Phys. Chem. Rare Earths*, vol. 25, pp. 101–264, 1998.
[40] X. Qin, X. Liu, W. Huang, M. Bettinelli, and X. Liu, ‘Lanthanide-Activated Phosphors Based on 4f-5d Optical Transitions: Theoretical and Experimental Aspects’, *Chem. Rev.*, vol. 117, no. 5, pp. 4488–4527, Mar. 2017, doi: 10.1021/acs.chemrev.6b00691.
[41] ‘(PDF) Quenching of the Eu3+ Luminescence by Cu2+ Ions in the Nanosized Hydroxyapatite Designed for Future Bio-Detection’. Accessed: Nov. 13, 2023. [Online]. Available: https://www.researchgate.net/publication/349286831_Quenching_of_the_Eu3_Luminescence_by_Cu2_Ions_in_the_Nanosized_Hydroxyapatite_Designed_for_Future_Bio-Detection
[42] J. Kaur, Y. Parganiha, and V. Dubey, ‘Luminescence Studies of Eu3+ Doped Calcium Bromofluoride Phosphor’, *Phys. Res. Int.*, vol. 2013, Jan. 2013, doi: 10.1155/2013/494807.